Chem, Volume *4*

Supplemental Information

Scalable and Sustainable Approach toward Highly Compressible, Anisotropic, Lamellar Carbon Sponge

Chaoji Chen, Jianwei Song, Shuze Zhu, Yiju Li, Yudi Kuang, Jiayu Wan, Dylan Kirsch, Lisha Xu, Yanbin Wang, Tingting Gao, Yilin Wang, Hao Huang, Wentao Gan, Amy Gong, Teng Li, Jia Xie, and Liangbing Hu

Supplementary Information

Supplemental Figures

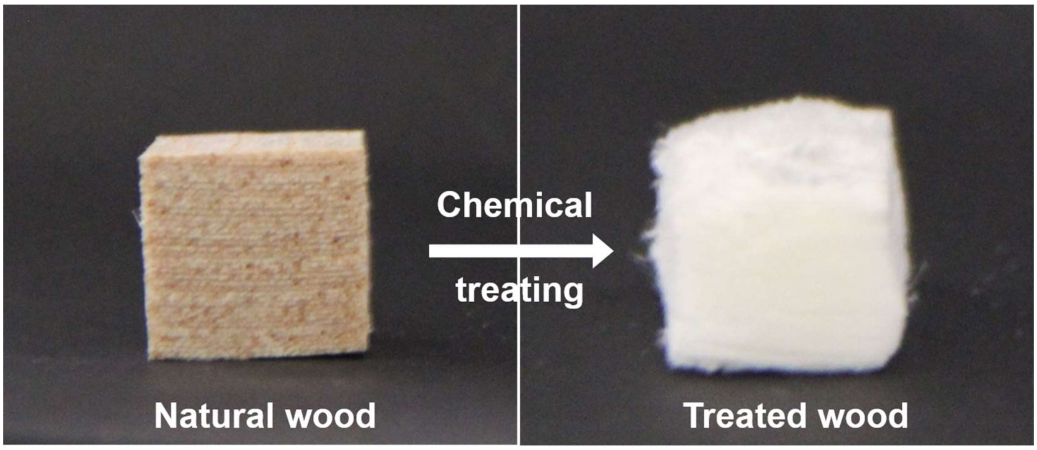

Figure S1. Photo Images of the Natural Wood and Treated Wood (Wood Sponge). It shows that the yellow natural wood becomes totally white after chemical treating due to the removal of lignin.

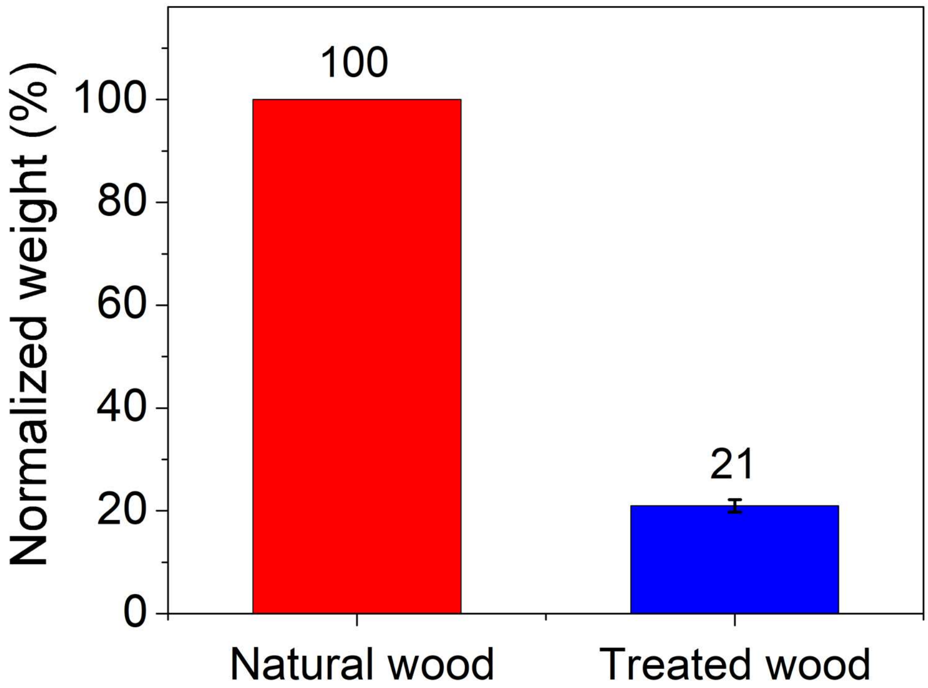

Figure S2. Weight Loss of the Wood Samples before and after Chemical Treatment. Error bars indicate standard deviations for 3 sets of data points.

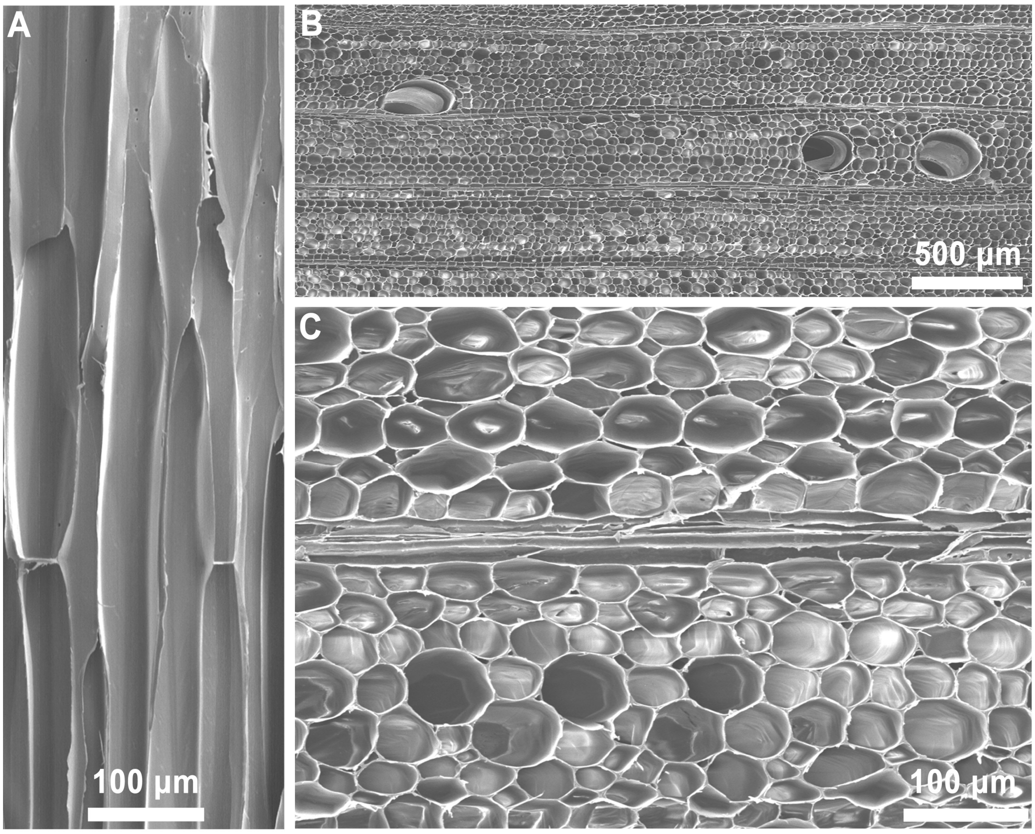

Figure S3. SEM Images of the Natural Balsa Wood. (A) Cross-section-view image, showing the channels along the growth direction. (B,C) Top-view images, showing the lattice-like structure of the natural wood with numerous channels.

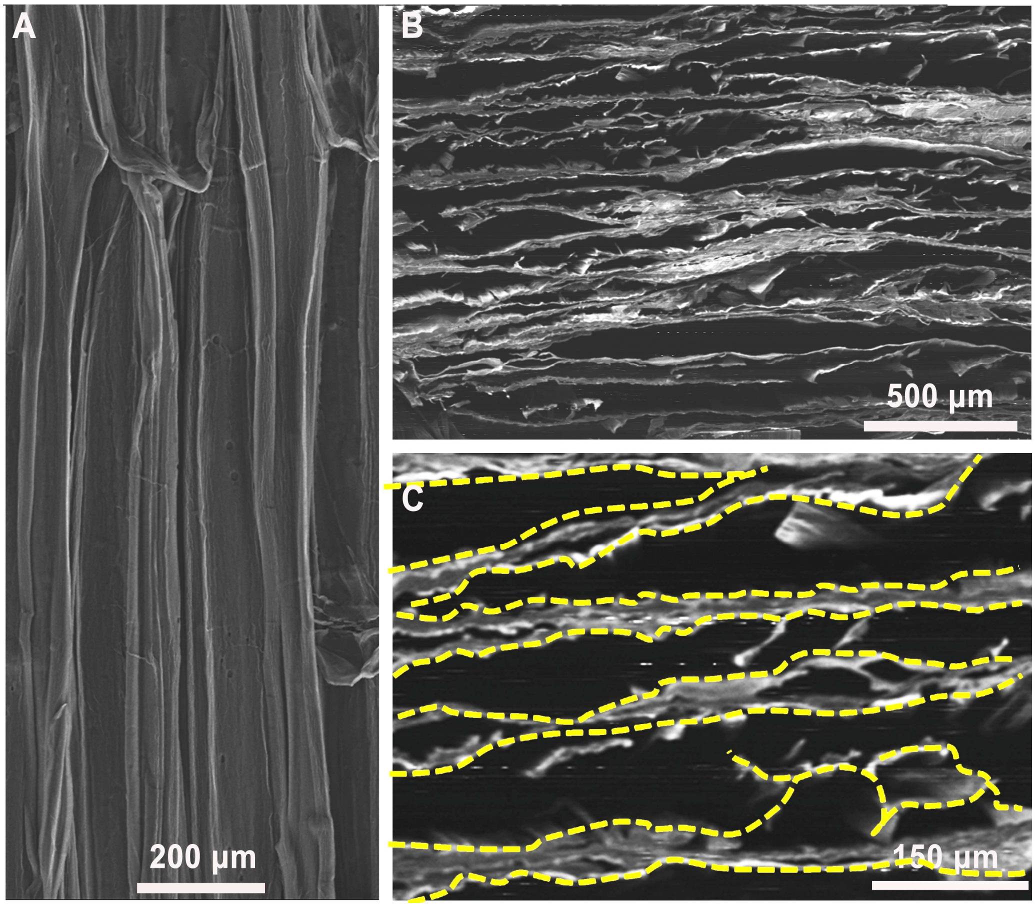

Figure S4. SEM Images of the Compressible Wood Sponge. (A) Cross-section-view image, showing that the channels along the growth direction become inconspicuous due to the chemical treating. (B,C) Top-view images, showing the lamellar structure comprised of numerous stacking curved layers.

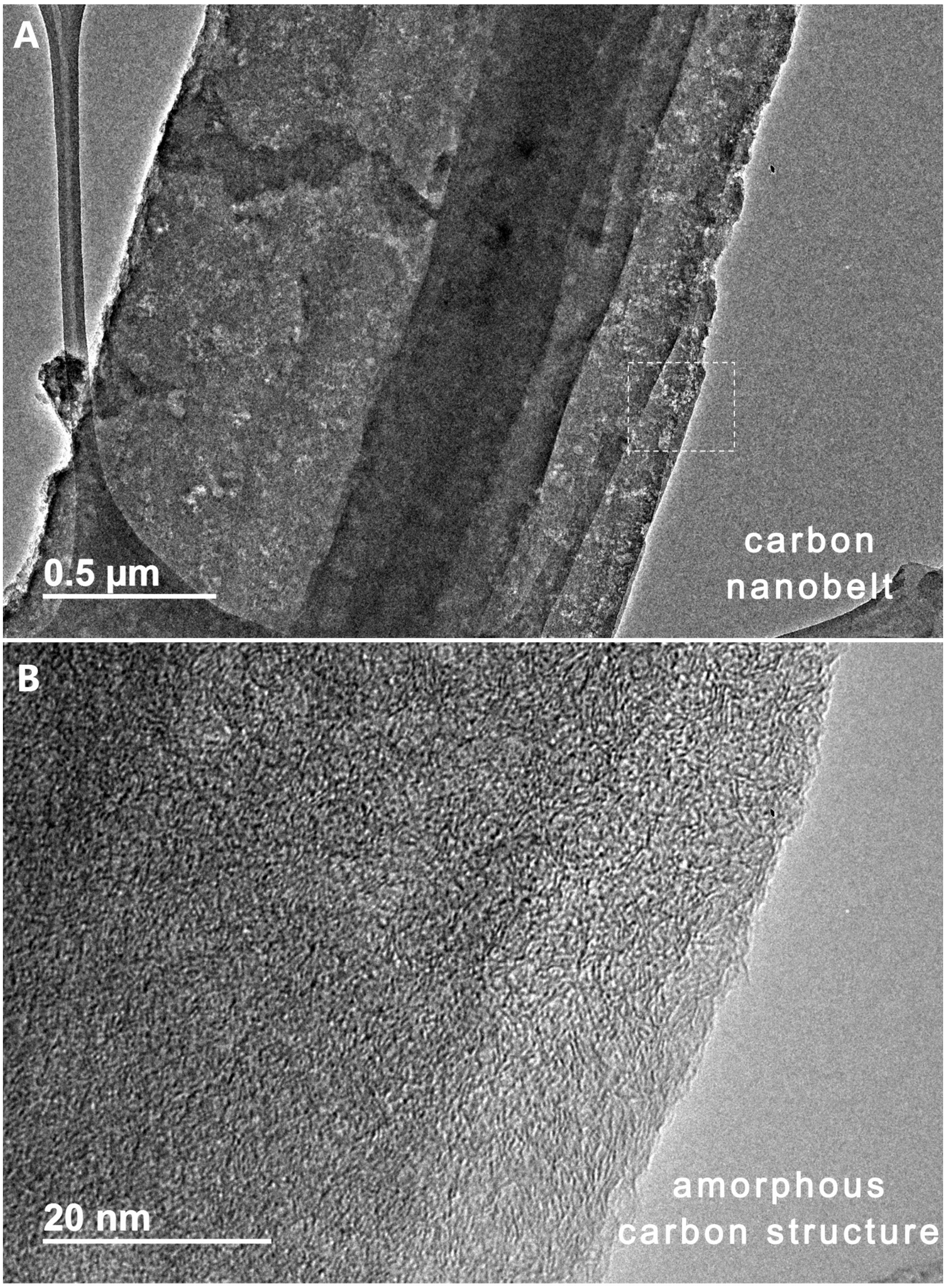

Figure S5. TEM and HR-TEM Images of the Wood Carbon Sponge. (A) TEM image. (B) HR-TEM image. Many disordered domains can be observed in the HR-TEM image, suggesting the wood carbon sponge has amorphous features.

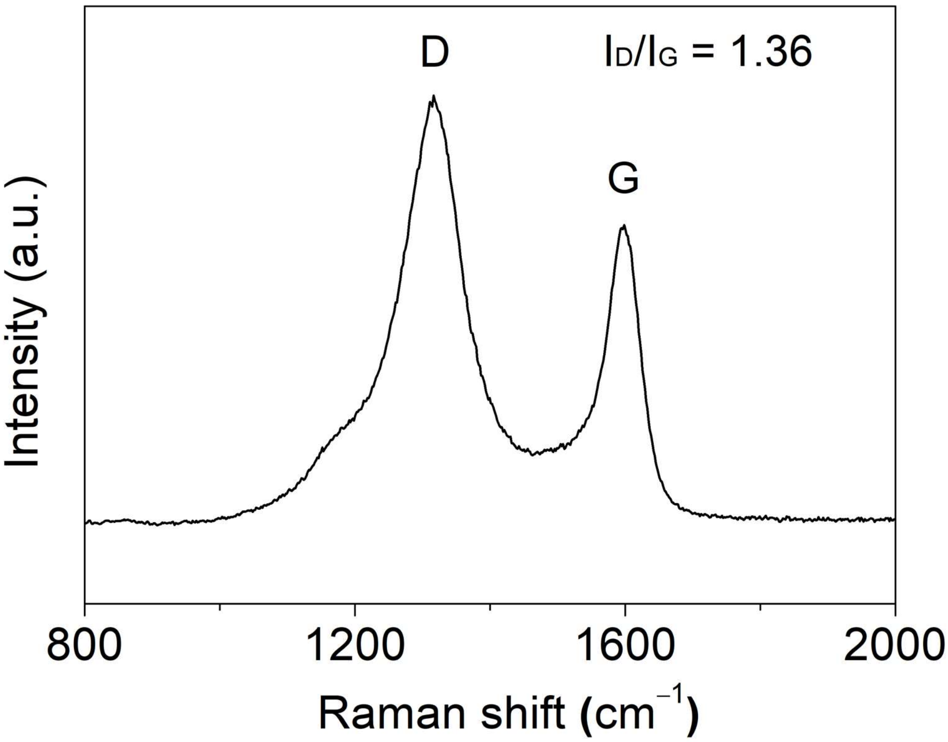

Figure S6. Raman Spectrum of the Wood Carbon Sponge. The obvious D and G peaks with a I_D/I_G value of 1.36 indicates the amorphous features of the wood carbon sponge.

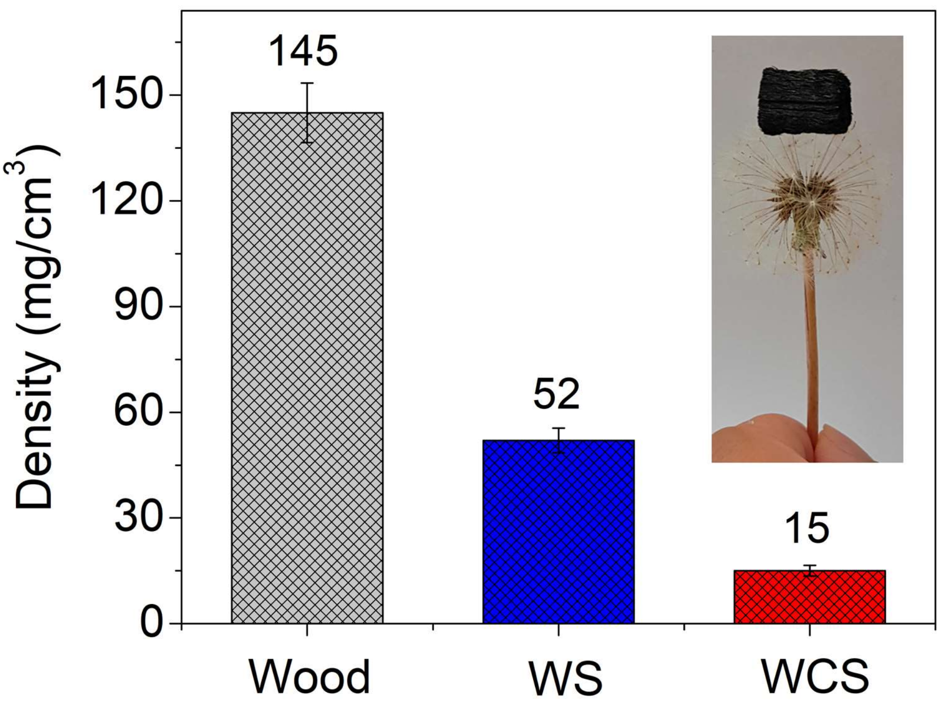

Figure S7. Density Evolutions from Natural Wood, to Wood Sponge (WS), and Wood Carbon Sponge (WCS). Inset shows the lightweight feature of the wood carbon sponge. Error bars indicate standard deviations for 3 sets of data points.

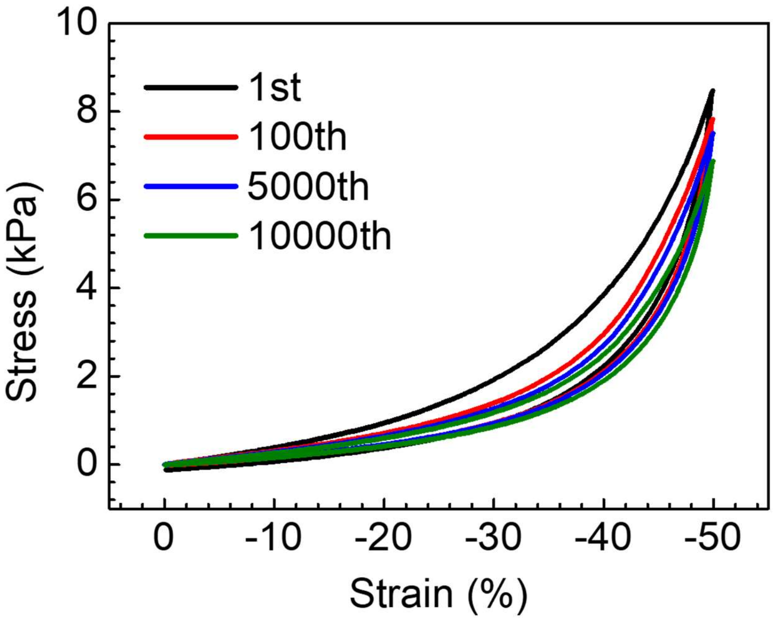

Figure S8. **Stress-Strain Curves of the WCS Obtained in Selected Cycles of 1st, 100th, 5000th, and 10000th.**

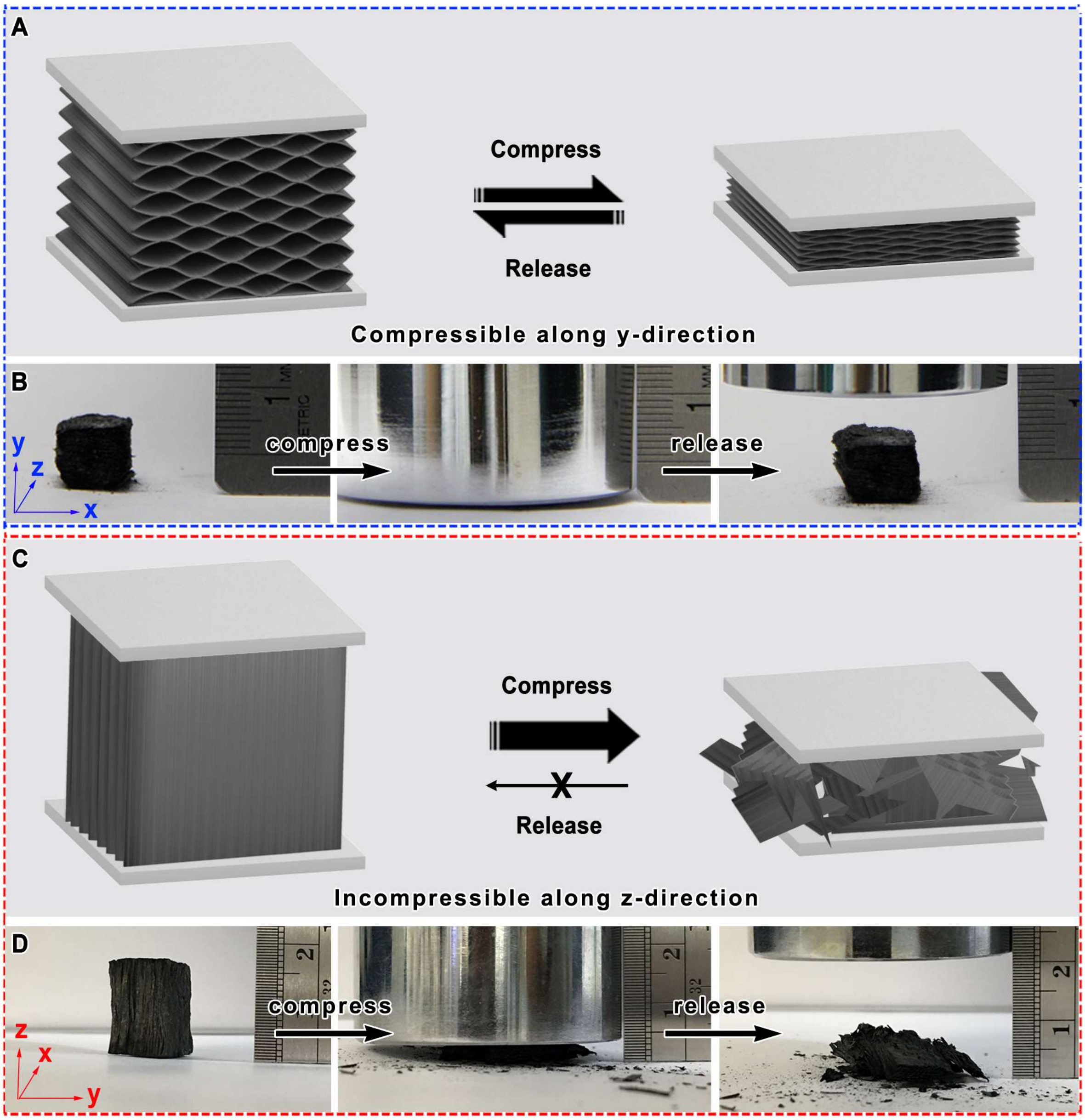

Figure S9. Anisotropic Mechanical Properties of the Wood Carbon Sponge. (A) Graphical illustration and (B) digital images of the compressible property of the wood carbon sponge along y-direction. (C) Graphical illustration and (D) digital images of the incompressible property of the wood carbon sponge along z-direction.

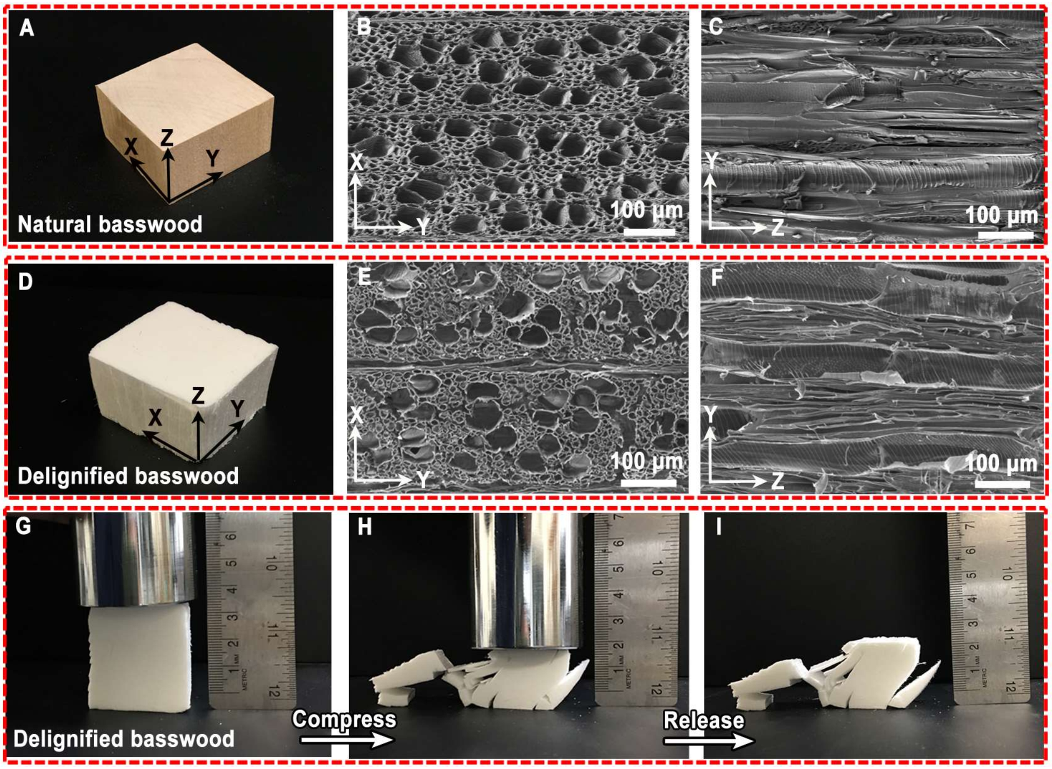

Figure S10. Structural Characterization of the Natural Basswood and Delignified Basswood. (A) Digital image of the natural wood. (B,C) SEM images of the natural basswood: (B) cross-sectional image showing the wood lumen structure (in XY plane); (C) longitudinal image showing the lumina along the growth direction (in YZ plane). (d) Photo image of the white basswood. (E,F) SEM images of the wood aerogel: (E) cross-sectional SEM image showing the structure in XY plane; (F) longitudinal SEM image showing the lumina along the growth direction (in YZ plane). (G-I) Photo images of the white basswood before compressing (G), under compression (H) and after recovery (I), respectively.

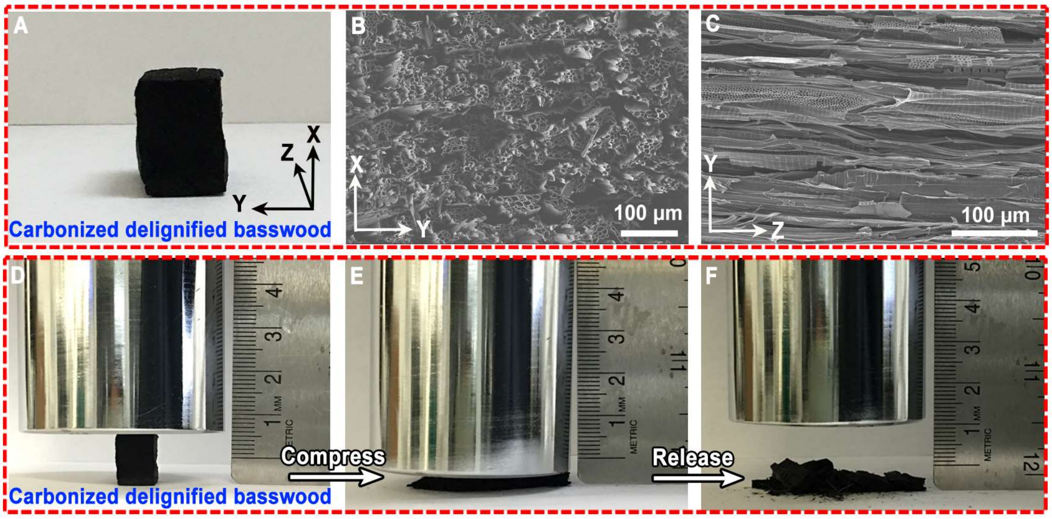

Figure S11. Structural Characterization of the Carbonized Delignified Basswood. (A) Digital image of the carbonized delignified basswood. (B,C) SEM images of the carbonized delignified basswood: (B) cross-sectional image showing the wood lumen structure (in XY plane); (C) longitudinal image showing the lumina along the growth direction (in YZ plane). (D-F) Digital images of the carbonized delignified basswood before compression (D), under compression (E) and after recovery (F), respectively.

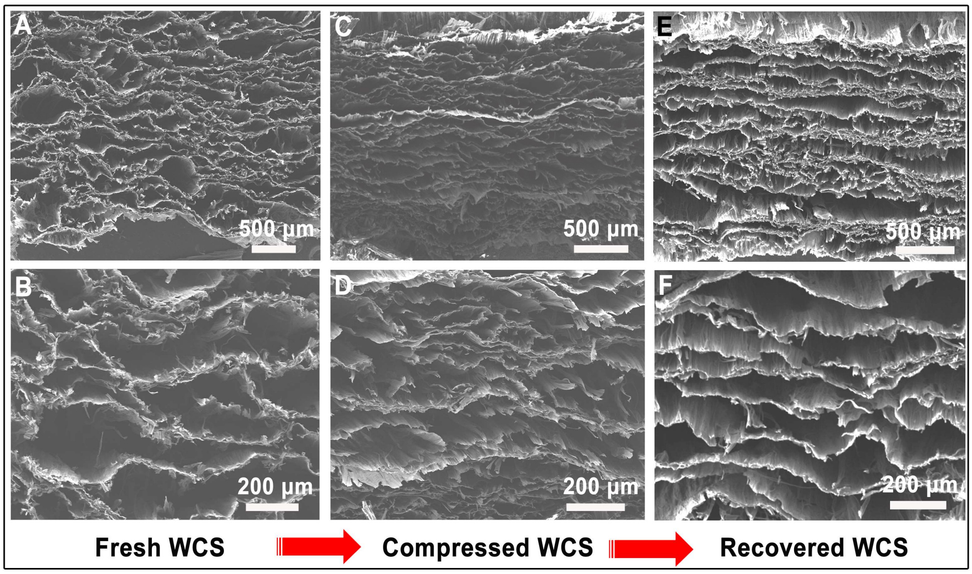

Figure S12. *Ex-situ* SEM Observations of the Wood Carbon Sponge. (A,B) Before compression. (C,D) During compression. (E,F) After releasing. Due to the arched layered structure, stress can be easily released by the small local bending of the arched layers, resulting in an excellent compressibility.

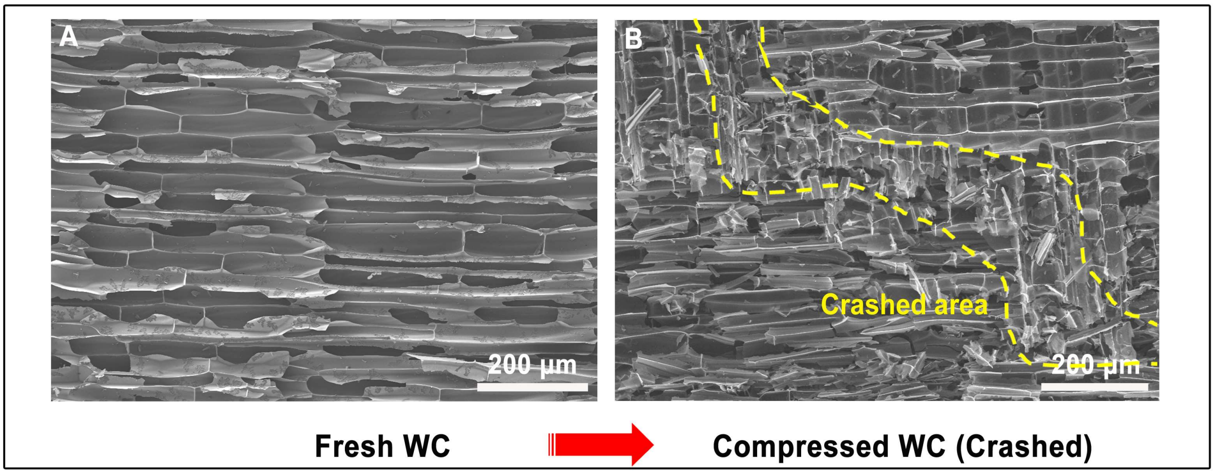

Figure S13. ***Ex-situ*** **SEM Observations of the Wood Carbon**. (A) Before compression. (B) After compression. The results show that the wood carbon, with a lattice-like structure, is easy to be crushed due to the stress concentrations at the cell merge points.

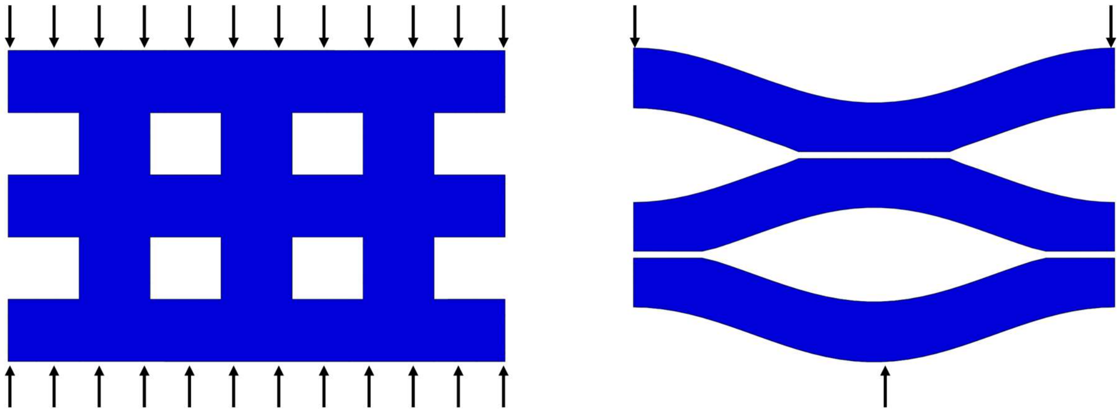

Figure S14. Finite Element Simulation Models of WC (Left) and WCS (Right).

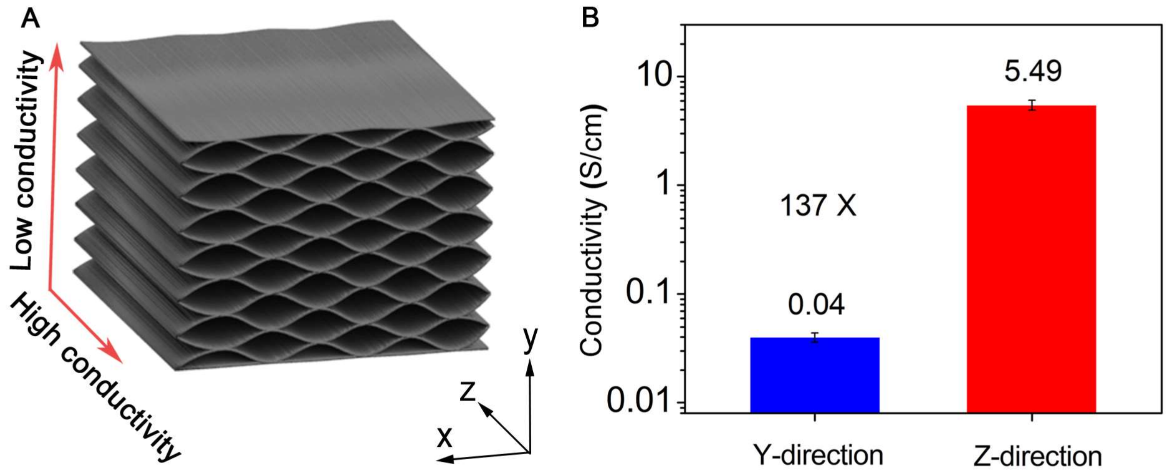

Figure S15. Anisotropic Electrical Properties of WCS. (A) Graphical illustration of the anisotropic structure and electrical conductivity of the wood carbon sponge. (B) Electrical conductivities of the wood carbon sponge along y- and z-directions with an anisotropic factor of ~137. Error bars indicate standard deviations for 3 sets of data points.

Supplemental Experimental Procedures

Characterizations:

The morphology and structure of materials were characterized by scanning electron microscopy (SEM, Hitachi SU-70), transmission electron microscopy (TEM, JEOL 2100F field-emission TEM) and X-ray diffraction (XRD, Rigaku Ultima III using Cu K α radiation (λ = 1.5406 Å)). Raman spectrum was collected on a commercial micro Raman spectrometer (Labram Aramis model manfuctured by Horiba Jobin Yvon). FT-IR spectrum was measured on a Thermo Nicolet NEXUS 670 FTIR. Compositional analysis was carried out on a high-performance liquid chromatography (HPLC) (Ultimate 3000, Thermo Scientific, USA). The mechanical compression test was performed on a universal testing machine (SHIMADZU AGS-X) with loading capacity from 0.01 to 170 N at a constant loading and unloading speed of 2 mm/min. For fatigue measurements at 50% strain for 10,000 cycles, the interval compression cycles were conducted by using a Dynamic Mechanical Analyzer (RSA 3, TA instruments) at 1 Hz. The electrical signals of the strain sensors were recorded at a Keithley 2400 digital meter at a constant voltage of 0.1 V.

Finite Element Simulations:

The finite element simulation is carried out using commercial code ABAQUS 6.10. The CPS4R, a 4-node bilinear plane stress quadrilateral element is used to mesh both the WCS model and the WC model. For the purpose of comparison, we keep the thickness of the channel walls in the WC structure model and the curved layers in the WCS structure model roughly the same, while strictly maintaining the same height (21.875 length unit), the same length (35 length unit), and same width (35 length unit) of the entire model. The mathematic description of the curved shape is a sinusoidal function, but it adopts a straight-line shape at the contact region between layers. Then an initial separation (0.5 length unit) between the curved layers is introduced in the WCS structure model for defining the contact between surfaces. Such a contact is modeled by using hard contact as the normal behavior and frictionless resistance as the tangential behavior. Displacement loading is applied as shown in **Figure S14**. The elastic properties are set as the following - Young's Modulus: 10 GPa, Poisson's ratio: 0.3.